The genetic architecture of language functional connectivity

Yasmina Mekki[a,*], Vincent Guillemot[b], Hervé Lemaitre[c], Amaia Carrion-Castillo[d], Stephanie Forkel[e,f,c], Vincent Frouin[a], Cathy Philippe[a,*]

[a] *Neurospin, Institut Joliot, CEA - Université Paris-Saclay, 91191 Gif-Sur-Yvette, France*
[b] *Hub de Bioinformatique et Biostatistique – Département Biologie Computationnelle, Institut Pasteur, USR 3756 CNRS, Paris, France*
[c] *Groupe d'Imagerie Neurofonctionnelle, Institut des Maladies Neurodégénératives, CNRS UMR 5293, Université de Bordeaux, Centre Broca Nouvelle-Aquitaine, Bordeaux, France*
[d] *Basque Center on Cognition, Brain and Language, San Sebastian, Spain*
[e] *Brain Connectivity and Behaviour Laboratory, Sorbonne Universities, Paris, France*
[f] *Department of Neuroimaging, Institute of Psychiatry, Psychology and Neurosciences, King's College London, UK*

Abstract

Language is a unique trait of the human species, of which the genetic architecture remains largely unknown. Through language disorders studies, many candidate genes were identified. However, such complex and multifactorial trait is unlikely to be driven by only few genes and case-control studies, suffering from a lack of power, struggle to uncover significant variants. In parallel, neuroimaging has significantly contributed to the understanding of structural and functional aspects of language in the human brain and the recent availability of large scale cohorts like UK Biobank have made possible to study language via image-derived endophenotypes in the general population. Because of its strong relationship with task-based fMRI activations and its easiness of acquisition, resting-state functional MRI have been more popularised, making it a good surrogate of functional neuronal processes. Taking advantage of such a synergistic system by aggregating effects across spatially distributed traits, we performed a multivariate genome-wide association study (mvGWAS) between genetic variations and resting-state functional connectivity (FC) of classical brain language areas in the inferior frontal (pars opercularis, triangularis and orbitalis), temporal and inferior parietal lobes (angular and supramarginal gyri), in 32,186 participants from UK Biobank. Twenty

*Corresponding author
Email addresses: yasmina.mekki@cea.fr (Yasmina Mekki), Cathy.PHILIPPE@cea.fr (Cathy Philippe)

genomic loci were found associated with language FCs, out of which three were replicated in an independent replication sample. A locus in 3p11.1, regulating *EPHA3* gene expression, is found associated with FCs of the semantic component of the language network, while a locus in 15q14, regulating *THBS1* gene expression is found associated with FCs of the perceptual-motor language processing, bringing novel insights into the neurobiology of language.

Keyword

Imaging-genetics, Resting-state functional MRI, Language, GWAS, UK Biobank, multivariate analysis

Abbreviations

rsfMRI, resting-state functional magnetic resonance imaging; FC, functional connectivity; GWAS, genome-wide association study; mvGWAS, multivariate GWAS; SNP, single nucleotide polymorphism; eQTL, expression quantitative trait locus;

1. Introduction

Language is a unique trait of the human species. Although its genetic origins are broadly accepted, they remain largely unknown. Since the seminal study that revealed the major role of *FOXP2* in language processing (Fisher et al., 1998), several candidate genes related to language disorders were identified (Landi and Perdue, 2019). Human language is a complex system – both structurally and functionally. As such a complex and multifactorial trait, it is unlikely to be associated with only a few genes but rather with many genes that are also interacting with each other. These genes likely contribute to the development of neural pathways involved in language development, together with experience-dependent contributions from the environment (Fisher and Vernes, 2015). In parallel, neuroimaging techniques provided innovative and quantitative ways to study language. Anatomically, the language system comprises perisylvian cortical regions predominantly - but not exclusively - in the left hemisphere. Amongst these regions the prominent regions are in the pars orbitalis and triangularis in the inferior frontal gyrus (also referred to as 'Broca's' region), the angular and supramarginal gyri in the inferior parietal lobe (also referred to as 'Geschwind's' region), and the posterior temporal regions ('Wernicke's' region). These cortical regions are interconnected by a network of brain connections, most prominently the arcuate fasciculus (Catani et al., 2005; Forkel and Catani, 2018). These regions also connect to the sensory-motor system (auditory, visual, and motor cortex). Functionally, phonology, semantics, and syntax are three main language components and form a tripartite parallel architecture (e.g. Jackendoff and Jackendoff (2002); Bates et al. (2003); Vigneau et al. (2006); Price (2012)). Consequently, it has become common practice to study language in the healthy population using neuroimaging. Mapping endophenotypes based on anatomical and task-based functional MRI expanded the understanding of how the brain supports language (Price, 2012; Friederici, 2017; Ardila et al., 2016; Leroy et al., 2015; Labache et al., 2020). These MRI endophenotypes give access to biologically relevant measurements of individual variability (Forkel et al., 2014a, 2020b; Uddén et al., 2019; Dubois and Adolphs, 2016; Seghier and Price, 2018; Fedorenko, 2021;

Forkel et al., 2020a) and are consequently suitable for the search of genetic associations. Traditionally, the language-brain relationship is investigated through task-based activation experiments. In the past decade, the use of resting-state functional MRI (rsfMRI) has been popularised mainly due to the strong relationship observed between the signals collected in resting-state and the cognitive task-based fMRI activations (Smith et al., 2009; Tavor et al., 2016; Cole et al., 2016; Ngo et al., 2020; Dohmatob et al., 2021). rsfMRI is paradigm free and as such it is easier to implement in very large cohorts like the UK Biobank. rsfMRI can recover specific brain functional activations making it a good surrogate of functional neuronal processes. Here, we propose to use task-free functional connectivity (FC) from the UK Biobank (Bycroft et al., 2018), using perisylvian cortical regions as areas of interest serving as a proxy for language.

As rsfMRI FC are low amplitudes and correlated to each other, we anticipate it would be really difficult to disentangle the genetic associations with each FC signal in a massively univariate manner. Language related brain regions share information across components and scales, and genetic variants are supposed to have distributed effect across regions. Thus, we take advantage of this synergistic system and perform a multivariate approach with MOSTest (van der Meer et al., 2020). This method considers the distributed nature of genetic signals shared across brain regions and aggregates effects across spatially distributed traits of interest. This approach tests each SNP independently for its simultaneous association with the brain endophenotypes, making it half multivariate and half univariate. For convenience, we will use the term "multivariate GWAS" (mvGWAS) while being aware that correlations between SNPs are not accounted for in this approach.

In this study, we use rsfMRI in a discovery sample of 32,186 healthy volunteers from the UK Biobank (Sudlow et al., 2015) and the compiled information of a large-scale meta-analysis on language components (Vigneau et al., 2006, 2011). First, we derived functional connectivity (FC) endophenotypes reflecting individual language network characteristics, based on regions of interest from the meta-analysis. Second, we performed a multivariate genetic asso-

ciation of language specific functional connectivity, filtered based on heritability significance. The results from this analysis were subjected to a replication study in an independent sample (N=4,754). Additionally, as the connections between different language regions are ensured by the white matter bundles (Catani et al., 2005; Catani and Forkel, 2019), we tested the potential associations of the hit SNPs with the neuroanatomical tracts underlying the hit endophenotypes using diffusion-based white matter analysis. Finally, the extensive functional annotations of each genomic risk locus allowed us to suggest two new genes with a role in different aspects of the language system.

2. Materials and Methods

2.1. Demographics and neuroimaging Data from the UK Biobank

UK Biobank cohort. The UK Biobank is an open-access longitudinal population-wide cohort study that includes 500k participants from all over the United Kingdom (Sudlow et al., 2015). Data collection comprises detailed genotyping and a wide variety of endophenotypes ranging from health/activity questionnaires, extended demographics to neuroimaging and clinical health records. All participants provided informed consent and the study was approved by the North West Multi-Centre Research Ethics Committee (MREC).

This study used the February 2020 release (application number #64984). This release consisted of 36,940 participants, age range between 40 to 70 years (mean age=54 $\pm$7.45 years), with genotyping and resting-state functional MRI. To avoid any possible confounding effects related to ancestry, we restricted our analysis to individuals with British ancestry using the sample quality control information provided by UK Biobank (Bycroft et al., 2018). A final cohort of 32,186 volunteers (15,234 females, mean age = 55 $\pm$7.51 years) were included in the study. We made use of the first ten principal components (Data field 22009) of the genotyping data's multidimensional scaling analysis capturing population genetic diversity to account for population stratification. An independent replication dataset of 4754 non-British individuals was also drawn from the UK Biobank. The age range of these participants was 40 to 70 (mean age = 53 $\pm$7.55 years), 2153 were female.

Resting-state functional MRI data. The MRI data available from the UK Biobank are described in the UK Biobank Brain Imaging Documentation (v.1.7, January 2020) as well as in (Miller et al., 2016; Alfaro-Almagro et al., 2018). Briefly, resting-state functional MRI (rsfMRI) data were acquired using the following parameters: 3T Siemens Skyra scanner, TR = 0.735s, TE = 39ms, duration = 6 min (490 time points), resolution: $2.4 \times 2.4 \times 2.4$ mm, Field-of-view = $88 \times 88 \times 64$ matrix. During the resting-state scan, participants were instructed to keep their eyes fixated on a crosshair, to relax, and to think of nothing particular

(Miller et al., 2016). The preprocessing of the UK Biobank data includes motion correction, grand-mean intensity normalisation, high-pass temporal filtering including EPI unwarping with alignment to the T1 template and gradient non-linearity distortion correction (GDC) unwarping, brain masking, and registration to MNI space. The rsfMRI volumes were further cleaned using ICA-FIX for automatically identifying and removing artefacts.

Diffusion-weighted MRI data. The Diffusion-weighted MRI (dMRI) images were acquired using the following parameters; isotropic voxel size (resolution): $2 \times 2 \times 2$ mm, five non diffusion-weighted image b=0 s/mm^2, diffusion-weighting of b=1000, and 2000 s/mm^2 with 50 directions each, acquisition time: 7 min. Tensor fits utilize the b=1000 s/mm^2 data and the NODDI (Zhang et al., 2012) (Neurite Orientation Dispersion and Density Imaging) model is fit using AMICO (Daducci et al., 2015) (Accelerated Microstructure Imaging via Convex Optimization) tool, creating outputs including nine diffusion indices maps. These ones were subject to a TBSS-style analysis using FSL tool resulting in a white matter skeleton mask.

2.2. Genetic quality control

Genotyping was performed using the UK BiLEVE Axiom array by Affymetrix (Wain et al., 2015) on a subset of 49,950 participants (807,411 markers) and the UK Biobank Axiom array on 438,427 participants (825,927 markers). Both arrays are extremely similar and share 95% of common SNP probes. The imputed genotypes were obtained from the UK Biobank repository Bycroft et al. (2018). These genetic data underwent a stringent quality control protocol, excluding participants with unusual heterozygosity, high missingness (Data field 22027), sex mismatches, such as discrepancy between genetically inferred sex (Data field 22001) and self-reported sex (Data field 31). Variants with minor allele frequency (MAF) < 0.01 were filtered out from the imputed genotyping data using PLINK 1.9 (Chang et al., 2015) to retain the common variants only. Overall, 9,812,367 autosomal SNPs were considered.

2.3. Regions of interest for rsfMRI functional connectivity

We leverage a large-scale meta-analysis of 946 activation peaks (728 peaks in the left hemisphere, 218 peaks in the right hemisphere) obtained from a meta-analysis of 129 task-based fMRI language studies (Vigneau et al., 2006, 2011). The identified fronto-parietal-temporal activation foci revealed via a hierarchical clustering analysis, 50 distinct, albeit partially overlapping, clusters of activation foci for phonology, semantics, and sentence processing: 30 clusters in the left hemisphere and 20 in the right hemisphere.

Because this overlap could unduly increase the co-activation between regions and to avoid a deconvolution bias in the estimation of the functional connectivity, we proceeded as follow: First, because the clustering process was performed for each component independently, we checked whether pairs of clusters belonging to different language-component networks were spatially distinct considering the significance of their mean Euclidean distance with paired t-tests. We identified areas that are common to multiple language components; in the temporal lobe, the anterior part of the Superior temporal gyrus (T1a) area appears to be common to all three language components, the anterior part of the superior temporal sulcus (Pole) and Lateral/middle part of the middle temporal gyrus (T2ml) are common to semantic and sentence's clusters and the posterior part of the left inferior temporal gyrus (T3p) to semantic and phonology clusters. In the frontal lobe, the L—R dorsal part of the pars opercularis (F3opd) and the ventral part of the pars triangularis (F3tv) are common to semantic and syntactic clusters. In these cases, we retained the larger cluster and assigned multiple labels. Second, ROIs were obtained for each cluster by building a 3D convex-hull of the peaks in the MNI space and were then subjected to a morphological opening operation. Third, overlapping areas between the convex-hull ROIs were processed as follows: the common region between two ROIs was attributed to the most representative in terms of the number of peaks. Finally, we excluded regions with less than 100 voxels. This preprocessing resulted in 25 multilabelled ROIs: 19 in the left hemisphere and 6 in the right hemisphere which are summarised in Fig. 1 and Table SI1.

2.4. Neuroimaging endophenotypes

Functional connectivity endophenotypes. The preprocessed resting-state BOLD signal was masked using the 25 ROIs and averaged at each time volume. A connectome matrix was computed using Nilearn (Abraham et al., 2014) for each participant using a shrunk (Ledoit and Wolf, 2004) estimate of partial correlation (Marrelec et al., 2006). This resulted in 300 ($= 25 \times 24/2$) edges connecting language ROIs for each individual. Each edge -also denoted functional connectivity (FC)- is further considered as a candidate endophenotype. See the Fig. 1b.

Diffusion MRI endophenotypes.

We hypothesised that the hit SNPs associated with the hit FCs could be associated with neuroanatomical white matter tracts that supports the information transmission between the regions that compose these hit-FCs. Therefore, we tested the potential associations between the hit SNPs with the following white matter bundles: the corpus callosum, the left frontal aslant tract, the left arcuate anterior/long/posterior segment, the left inferior fronto-occipital fasciculus, the left uncinate tract (See section 3.3 for more details). The resulting skeletonised images are averaged across the set of 7 brain white matter structures defined by the probabilistic atlas (Rojkova et al., 2016) thresholded at 90% of probabilities. These structural white matter tracts are assessed by 9 indices: fractional anisotropy (FA) maps, tensor mode (MO), mean diffusivity (MD), intracellular volume fraction (ICVF), isotropic volume fraction (ISOVF), mean eigenvectors (L1, L2, L3), and orientation dispersion index (OD) yielding $63 = 7 \times 9$ dMRI endophenotypes.

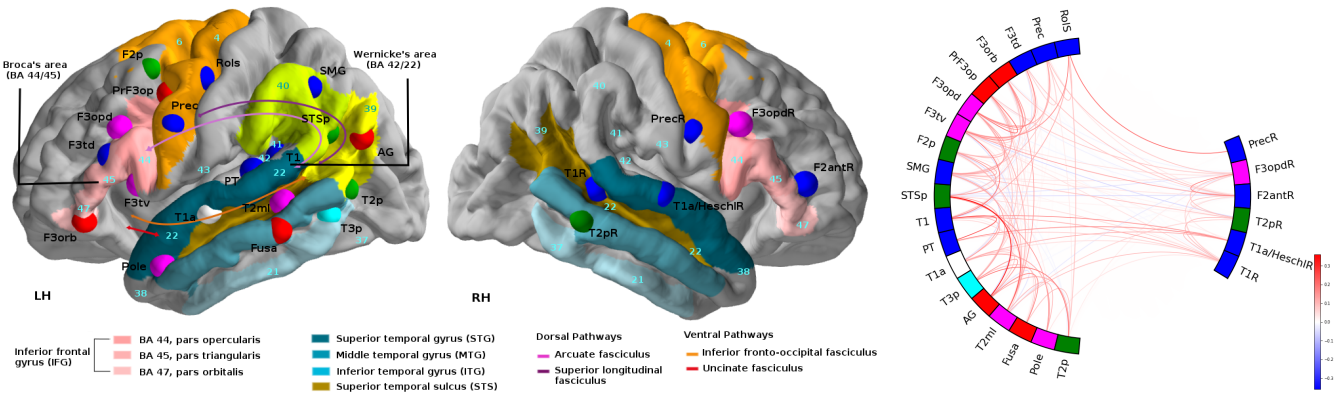

Figure 1: A) Overview of the regions obtained from the meta-analysis. Each language seed is color-coded according to its language category: phonology (blue), semantic (red), and syntax (green). ROIs of different components that were not spatially distinct are color-coded as pink (semantic/syntax), cyan (phonology/semantic) and white for the three language component. For the sake of ROIs figure visibility, the coordinates were modified. The exact coordinates for each ROI are available in Table **??**. Different gyri and sulcus, known to be relevant for language: the inferior frontal gyrus (IFG), middle temporal gyrus (MTG), superior temporal gyrus (STG), and superior temporal sulcus (STS), are color-coded. Numbers in the left hemisphere (LH) represents language-relevant Brodmann areas (BA) which were defined on the basis of cytoarchitectonic characteristics. Numbers in the right hemisphere (RH) represents the language-relevant BA counterpart. The pars opercularis (BA 44), the pars triangularis (BA 45) represents Broca's area. The pars orbitalis (BA 47) is located anterior to Broca's area. BA 42 and BA 22 represents Wernicke's area Friederici (2011). Both supramarginal gyrus (BA40) and angular gyrus (BA39), also known as Geschwind's territory, are represented by green/yellow colors respectively. The primary motor cortex (BA4), the premotor cortex and the supplementary motor area (B6) are colored in orange. Whitin the left hemisphere, dorsal and ventral long-range fiber bundles connect language areas and are indicated by color-coded arrows. B) Mean functional connectivity of the 142 heritable endophenotypes, calculated using a shrinked estimate of partial correlation Marrelec et al. (2006) (estimated with a Ledoit-Wolf estimator Ledoit and Wolf (2004)) over 32,186 UKB rs fMRI subjects.

2.5. SNP-based heritability and genetic correlation analysis.

The proportion of additive genetic variance in the FC phenotypic variance, also called narrow-sense heritability, was estimated using the genotyped SNPs information using genome-based restricted maximum likelihood (GREML) (Yang et al., 2010) for each FCs, controlling for the above-mentioned covariates (refer to section 2.4). To define significantly heritable FCs, a 0.05 threshold on False Discovery Rate (FDR) adjusted p-values was applied to account for multiple testing on the 300 FCs. Similarly, the proportion of additive genetic variance in the covariance of pairs of FCs was estimated using the bivariate GREML (Lee et al., 2012). Both heritability and part of covariance explained by genetics were obtained using GCTA (Yang et al., 2011).

2.6. Multivariate genome-wide association studies (mvGWAS)

We performed a multivariate genome-wide association studies (mvGWAS) between the filtered imputed genotypes and the 142 significantly heritable FC endophenotypes, using the Multivariate Omnibus Statistical Test (MOSTest) (van der Meer et al., 2020). All endophenotypes were pre-residualised controlling for covariates including sex, genotype array type, age, recruitment site, and ten genetic principal components provided by UK Biobank. In addition, MOSTest performs a rank-based inverse-normal transformation of the residualised endophenotypes to ensure that the inputs are normally distributed. The distributions across the participants of all endophenotypes were visually inspected before and after covariate adjustment. MOSTest generated summary statistics that capture the significance of the association across all heritable 142 language FC endophenotypes. To account for multiple testing over the whole genome, statistically significant SNPs were considered as those reaching the genome-wide threshold $p = 5e{-}8$.

2.7. mvGWASes replication

The multivariate genome-wide association results were replicated in an independent non-British sample considering the nominal significance threshold $p < 0.05$. Following the same pre-processing steps as for the primary sample, the non-British replication sample consists in 4,754 individuals with a mean age of 53 years ($\pm$7.55) and 2,153 female.

2.8. Fine-mapping: identification of genomic risk loci and functional annotation

We performed functional annotation analysis using the FUMA online platform v1.3.6a (Watanabe et al., 2017) with default parameters. The genomic positions are reported according to the GRCh37 reference. SNPs were annotated for functional consequences on gene functions using ANNOVAR (Wang et al., 2010), Combined Annotation Dependent Depletion (CADD) scores (Kircher et al., 2014), and 15-core chromatin state prediction by ChromHMM (Ernst and Kellis, 2012). In addition, they were annotated for their effects on gene expression

using eQTLs of various tissue types. The eQTL module queried data from different tissue-datasets using GTEx v8 (Consortium et al., 2017), Blood eQTL browser (Westra et al., 2013), BIOS QTL browser (Zhernakova et al., 2017), BRAINEAC (Ramasamy et al., 2014), eQTLGen (Võsa et al., 2018), PsychENCODE (Wang et al., 2018), DICE (Schmiedel et al., 2018). RegulomeDB v2.0 (Boyle et al., 2012) was queried externally. Coding hit SNPs are also annotated with polymorphism phenotyping v2 (Polyphen-2) (Ramensky et al., 2002).

3. Results

3.1. SNP-based heritability of functional connectivity measures

The single-nucleotide polymorphism (SNP)-based heritability (h^2) was estimated for each of the 300 FCs endophenotypes. P-values correction for multiple testing revealed 142 FCs significant SNP-based heritabilities (Table SI2), ranging from 14% for the SMG↔F3opd to 3% for the SMG↔T1 FC.

3.2. Multivariate genome-wide association analysis

We performed a multivariate genome-wide association study (mvGWAS) using the Multivariate Omnibus Statistical Test (MOSTest) (van der Meer et al., 2020) method, with the 142 FCs with significant SNP-based heritability. This analysis tested each SNP separately for its simultaneous association with the 142 FCs and yielded 4566 significant SNPs at a genomic threshold (see Table SI3), distributed on chromosomes 2, 3, 5, 6, 10, 11, 14, 15, 17, 18 and 22. FUMA (Watanabe et al., 2017) software was used to analyse mvGWAS results and identify lead SNPs at each associated locus. Considering the genome-wide significance threshold $p = 5e{-}8$, there were 20 distinct genomic loci distributed on the 11 chromosomes, associated with different aspects of language FC (Fig.2a, Table 1 and Fig. SI1, SI2, 2b, and SI3) and represented by 20 lead SNPs.

Validation of lead SNPs associated with rsfMRI FCs. The three lead SNPs were replicated at the nominal significance level ($p < 5e{-}2$) on multivariate test in the independent non-British replication dataset: $rs1440802(p = 9.58e{-}3)$, $rs35124509(p = 3.25e{-}3)$,

$rs11187838(p = 2.92e{-}2)$. Table SI4 summarises these results. Moreover, these lead SNP showed association at $p < 0.05$ on univariate testing of all but three specific central traits identified in the discovery mvGWAS.Here, we present three of these loci that were replicated in an independent data set (refer to section 2.3). MOSTest results highlighted the three following genomic risk regions: *i)* 15q14 locus (chr15, start=39598529, length=260kb) with its strongest association related to the imputed SNP rs1440802 ($p = 1e{-}31$); *ii)* 3p11.1 locus (chr3, start=89121389, length=1,381kb) with its strongest association related to the imputed SNP rs35124509 ($p = 8.95e{-}59$); *iii)* 10q23.33 locus (chr10, start=95988042, length=139kb) with its strongest association related to the imputed SNP rs11187838 ($p = 4.29e{-}14$). See Fig. 2a and Table 1.

Identification of central endophenotypes associated with genomic risk regions. For each lead SNP, we defined the 'central' endophenotypes that contributed the most in the multivariate association by using the individual univariate summary statistics performed by MOSTest and by considering the genome-wide significance threshold ($p < 5e - 8$) (Table SI5).

On 15q14, the lead SNP rs1440802 had two central FCs: the minor allele was associated with the partial correlation between *i)* the precentral gyrus and the dorsal pars opercularis (Prec↔F3opd). Both connected regions are in the left frontal lobe, and are labelled with a phonological linguistic component (Prec) and multi-labelled with semantic and sentence language processing (F3opd). *ii)* The (PrecR↔RolS) corresponds to the partial correlation between the precentral gyrus and the Rolandic sulcus. Both regions are identified in the right and left frontal lobes respectively, and are labelled as phonological linguistic component (Fig. 3a and Table SI5). These edges have previously been described in FC studies dedicated to language and more specifically in the perceptual motor interactions (Schwartz et al., 2008; Fridriksson et al., 2009; Turner et al., 2009; Nishitani and Hari, 2000; Schwartz et al., 2012). At the univariate level, these loci associated to central endophenotypes display an important overlap; See Fig 3d.

On 3p11.1, the lead SNP rs35124509 had nine central FCs: the minor allele was associated with the partial correlation between the left posterior part of the superior temporal sulcus and the left temporal pole (Pole↔STSp), the left temporal pole and the lateral/middle part of the middle temporal gyrus (Pole↔T2ml), the angular gyrus and the pars orbitalis of the left inferior frontal gyrus (AG↔F3orb), the anterior part of the Superior temporal gyrus and the left posterior part of the superior temporal sulcus (T1a↔STSp), the left posterior part of the superior temporal sulcus and the pars orbitalis of the left inferior frontal gyrus (STSp↔F3orb), the supramarginal gyrus and the posterior part of the left inferior temporal gyrus (SMG↔T3p), the angular gyrus and the left posterior part of the superior temporal sulcus (AG↔STSp), the Posterior part of the middle frontal gyrus and the angular gyrus (F2p↔AG), the lateral/middle part of the middle temporal gyrus and the supramarginal gyrus (T2ml↔SMG) (Fig. 4a and Table SI5). These connected regions are located across the left parieto-frontal-temporal lobe, and are mainly labelled as semantic language processing. These edges have previously been described in FC studies dedicated to language and especially to the semantic component. This component typically includes the inferior frontal gyrus, the left temporal cortex (i.e. temporal pole, middle temporal gyrus, fusiform gyrus) and the left angular gyrus (Binder et al., 2009; Jackson et al., 2016; Vigneau et al., 2006). At the univariate level, these loci associated to central endophenotypes display an important overlap; See Fig 4d.

A locus in 10q23.33 was highlighted by the mvGWAS. At the univariate level, no endophenotype reached the genome-wide significance threshold for the leas SNP in this locus (rs11187838).

As a conclusion of the mvGWAS, we retained: *i)* a multifold link between two FCs and a locus in 15q4 region; and *ii)* a multifold link between nine FCs and a locus in 3p11.1 region. Such a multivariate approach has the advantage of leveraging the distributed nature of genetic effects and the presence of pleiotropy across endophenotypes. Loci respectively identified by MOSTest as associated with several FCs made clear that these SNPs have distributed effects,

often with mixed directions, across regions and FCs. Fig. **??**b shows the FCs associations with both 15q14, and 3p11.1 lead SNPs. The regional effects of all other lead SNPs can be appreciated in the Supplementary Fig. **??**.

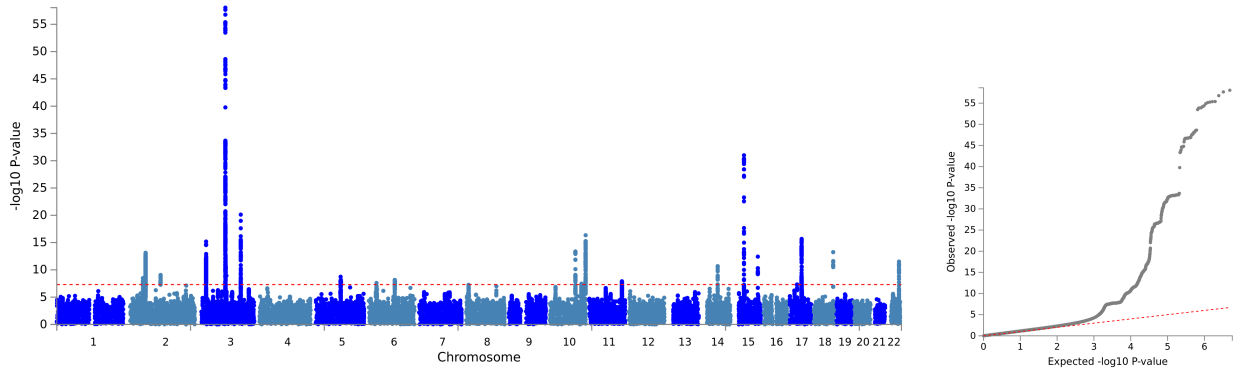

A)

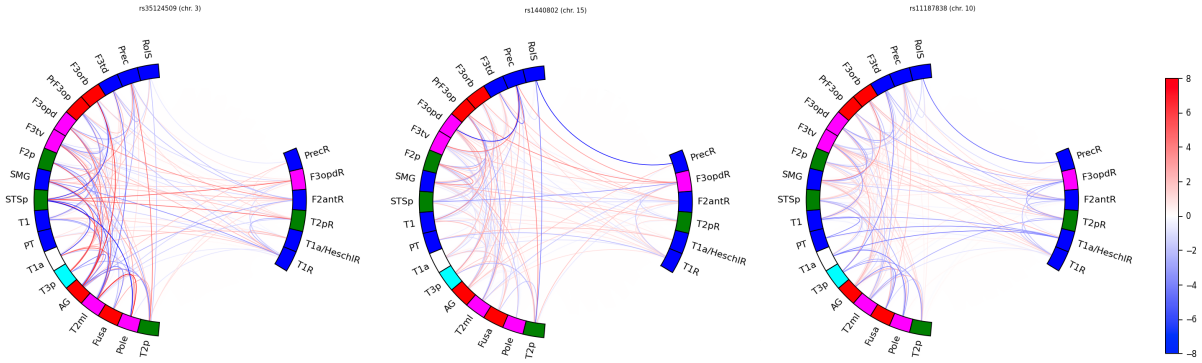

B)

Figure 2: A) Multivariate GWAS analysis of the resting state functional connectivity in 32,186 participants. Manhattan plot for multivariate GWAS accross 142 FCs. The red dashed line indicates the genome-wide significance threshold $p = 5e{-}8$. The Quantile-quantile plot is also shown. B) Circle plot illustrating the 3 lead SNPs identified from the mvGWAS. Z-values from the univariate GWAS for each FC are mapped. The absolute Z-values scaling is clipped at 8 ($p = 1.2e{-}15$). Positif effects of carrying the minor allele are shown in red, and negative in blue.

3.3. Downstream analyses

SNP-based genetic correlation of functional connectivity measures The SNP-based genetic correlation analysis was estimated (using GCTA (Lee et al., 2012) software) for each pair of central FCs associated to 15q14 or 3p11.1 genetic loci, indicating overlapping genetic contributions among several FCs (Table SI6). For central endophenotypes associated

with 3p11.1 locus, a negative genetic correlation between some FCs has been observed which indicates that variants can have antagonistic effects on the co-activations of these regions.

Validation of lead SNPs using diffusion imaging derived endophenotypes. We hypothesised that the genetic variants significantly associated with the language FCs could be associated with neuroanatomical tracts that support the information transmission between language areas. Therefore, we tested the potential associations between the hit SNPs with the average values of dMRI relevant white matter tracts :

3 white matter tracts to be tested with locus on 15q14: the white matter tracts linking the regions of the (Prec↔F3opd) consists of the *i)* arcuate anterior segment fasciculus (AF) dorsal pathway (Catani et al., 2005), *ii)* the frontal aslant tract (FAT) which is reported as connecting Broca's region (BA44/45) with dorsal medial frontal areas including supplementary and pre-supplementary motor area (BA6) (Rojkova et al., 2016; Catani and Forkel, 2019) while the anatomical connectivity underlying the (PrecR↔RolS) FC endophenotype consists of the corpus callosum which interconnects both hemispheres.

5 white matter tracts to be tested with locus on 3p11.1: the nine central endophenotypes associated with the 3p11.1 locus, the anatomical connectivity underlying these connections consists of the *i)* inferior fronto-occipital fasciculus (IFOF) which connects the inferior frontal regions with the temporal and occipital cortex (Forkel et al., 2014b), *ii)* uncinate fasciculus (UF) which is reported to connect the anterior temporal lobe to the orbital region and part of the inferior frontal (Vigneau et al., 2006; Catani and De Schotten, 2008; Friederici, 2017; Catani and Forkel, 2019), and the *iii)* arcuate long/anterior/posterior segment fasciculus (AF) (Catani et al., 2005).

As the anterior segment of AF is tested with both loci, this yields a Bonferroni-corrected threshold of $p = 6.94\text{e}{-3}(0.05/(3*9+5*9))$ (Table SI7). The MO measured in the FAT and the OD measured in the anterior segment of AF are associated with the rs1440802 SNP with $p = 3.33\text{e}{-6}$ and $p = 2.47\text{e}{-65}$, respectively. The corpus callosum exhibits no significant association. The MO measured in the IFOF and UF is associated with the rs35124509 SNPs

with $p = 2.49e{-}7$ and $p = 2.12e{-}7$, respectively. Both long and posterior segment of AF are associated with rs35124509 SNPs with $p = 5.88e{-}6$ (OD) and $p = 3.90e{-}7(L3)$, while the anterior segment of AF exhibits no significant association (See Table SI7).

3.4. Functional annotations of genomic loci associated with language

Locus in 15q14 associated to (Prec↔F3opd) and (PrecR↔RolS) endophenotypes. Four independent SNPs were identified in locus 15q14 (rs1440802, rs11629938, rs773225188, rs34680120) (Fig. 3c). Regarding eQTL annotations, we explored tissue-specific gene expression resources, including both brain tissues and blood - considered as a good proxy when brain tissues are not available (Qi et al., 2018). Significant results were obtained:

The four independant SNPs are cis-eQTL of *THBS1* gene in eQTLGen, BIOSQTL and GTEx/v8 . Additionally, rs34680120 is eQTL of *RP11-37C7.1* gene ($p_{adj} < 1.02e{-}3$) in PsychENCODE and eQTL of *CTD-2033D15.1* gene ($p_{adj} < 6.0e{-}6$) in BIOSQTL; see Fig.3c. Overall, the variants of this genomic risk region are found 72 times as eQTL of genes from different data sources. All eQTL associations are presented in more detail in Table SI8. Based on the human gene expression data from the Brainspan database, we found that *THBS1* gene has relatively high mRNA expression during early mid-prenatal to late prenatal stages, from 16 to 37 post-conceptional weeks; see Fig. 3e. Indirect predictions might be added from the following annotation. *RASGRP1*, identified by chromatin interaction mapping and which also appears to be under control of temporal expression during neurodevelopment, is reported as over-expressed in the perisylvian language areas (Johnson et al., 2009) and as up-regulated in the dorsal striatum (Cirnaru et al., 2020). Fig. 3 summarises these results, found by mvGWAS, associated to (Prec↔F3opd) and (PrecR↔RolS) FC endophenotypes. These pinpoint *THBS1* as the possible gene underlying this association signal.

Locus in 3p11.1 associated to semantic-language related endophenotypes. Fourteen independent SNPs were identified in locus 3p11.1 (Fig. 4c). The rs35124509 SNP is a non-synonymous variant within exon 16 of *EPHA3* protein-coding gene. The subregion

around rs35124509 and rs113141104 has its chromatin state annotated as (weak) actively-transcribed states (Tx, TxWk) in the brain tissues, specifically in the Brain Germinal Matrix, the Ganglion Eminence derived primary cultured neurospheres, and in the Fetal Brain Female. Concerning the subregion around rs6551410, it has its chromatin state annotated as Weak transcription (TxWk) in the Fetal Brain Female, enhancer (enh) in the Brain Germinal Matrix and Repressed PolyComb (ReprPC) in both the Ganglion Eminence and Cortex derived primary cultured neurospheres. Additionally, the subregion around rs6551407 has its chromatin state annotated as Weak transcription (TxWk) in the Brain Germinal Matrix, Fetal Brain Male and Fetal Brain Male. Overall, this reveals a genomic region involved in fine regulation mechanisms of brain development.

Considering the rs35124509 SNP and variants in linkage disequilibrium (LD) with it in the genomic risk region, we scrutinised CADD and RDB scores, precise genomic positions and risk prediction, and we noticed some remarkable SNPs. We observed two exonic variants: *i)* The SNP rs1054750 ($LD_{rs35124509}$ $r^2 > 0.99$, $p_{mvGWAS} = 6.65e-34$) is a synonymous variant within exon 16 of *EPHA3*. *ii)* the already mentioned non-synonymous lead SNP rs35124509 ($p_{mvGWAS} = 8.95e-59$), the minor allele results in a substitution in the protein from tryptophan (W) residue (large size and aromatic) into an arginine (R) (large size and basic) at position 924 (W924R, p.Trp924Arg) in the Sterile Alpha Motif (SAM) domain. This SNP is not predicted to alter protein function (Polyphen-2 = "benign") but is predicted to be potentially a regulatory element by several tools (RDB score = $3a$, CADD = 22.3 - when $\text{CADD}_{thresh} = 12.37$ for deleterious effect as suggested by Kircher et al. (2014)) Moreover, we observed eight SNP (rs28623022, rs7650184, rs7650466, rs73139147, rs3762717, rs73139144, rs73139148, rs566480002) ($LD_{rs35124509}$ $r^2 > 0.73$, $p_{mvGWAS} < 4.46e-20$) located in 3'-UTR of *EPHA3* which could affect its expression by modulating miRNA binding (Popp et al., 2016). The hit-SNP rs35124509 and the rest of highlighted SNPs act as eQTL for *EPHA3* in different tissues including brain cerebellum ($p_{FDR} < 5e{-}2$ in GTEx/v8 data source). The exhaustive eQTL associations are presented in Table SI8. Fig. 4 summarises the functional

annotations in 3p11.1 associated to multiple FC endophenotypes in semantic component of language. These functional characterization supports *EPHA3* as a possible gene with a key role in language development in humans.

Locus in 10q23.33. Four independent SNPs were identified in locus 10q23.33 (rs11187838, rs17109875, rs11187844, rs20772180). The subregion around all four SNPs has its chromatin state annotated as (weak) actively-transcribed states (Tx, TxWk) in the brain tissues, specifically in the ganglion eminence and cortex derived primary cultured neurospheres, hippocampus (middle), substantia nigra, anterior caudate, angular gyrus, Dorsolateral/Prefrontal cortex, brain germinal matrix, fetal brain female/male and NH-A astrocytes primary cells. Two exonic variants are noteworthy: The rs2274224 ($LD_{rs11187838}$ $r^2 > 0.99$, $p_{mvGWAS} = 5.04e-14$) and rs11187895 ($LD_{rs17109875}$ $r^2 > 0.6$, $p_{mvGWAS} = 3.08e-7$) SNPs are nonsynonymous SNV within exon 19 of *PLCE1* and exon 11 of *NOC3L* and are both not predicted to alter protein function (Polyphen-2="benign") but are predicted to have a deleterious effect (CADD = 17.35, CADD = 19.24). Moreover, we observed three SNP (rs11187870, rs11187877, rs145707916) ($LD_{rs17109875}$ $r^2 > 0.66$, $p_{mvGWAS} < 7.546e-7$) located in 3'-UTR of *PLCE1:NOC3L*. Regarding eQTL annotations, the variants in the 10q23.33 locus act as eQTL for *HELLS*, *NOC3L* and *PLCE1* genes in different brain tissues including brain cerebellum, brain cerebellar hemisphere, Brain nucleus accumbens basal ganglia, hippocampus ($p_{FDR} < 5e{-}2$ in GTEx/v8 data source). The exhaustive eQTL associations are presented in Table SI8. These functional characterisation highlight these three genes (*HELLS*, *NOC3L* and *PLCE1*) that may influence the FCs related to language processing in humans.

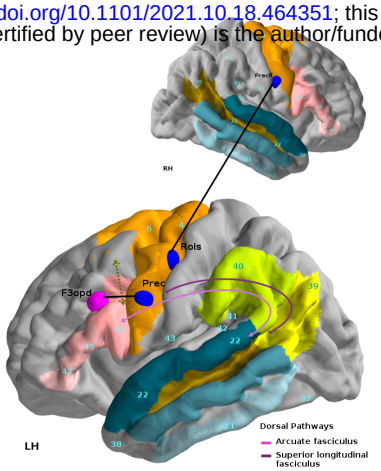

A)

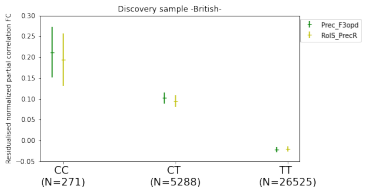

B)

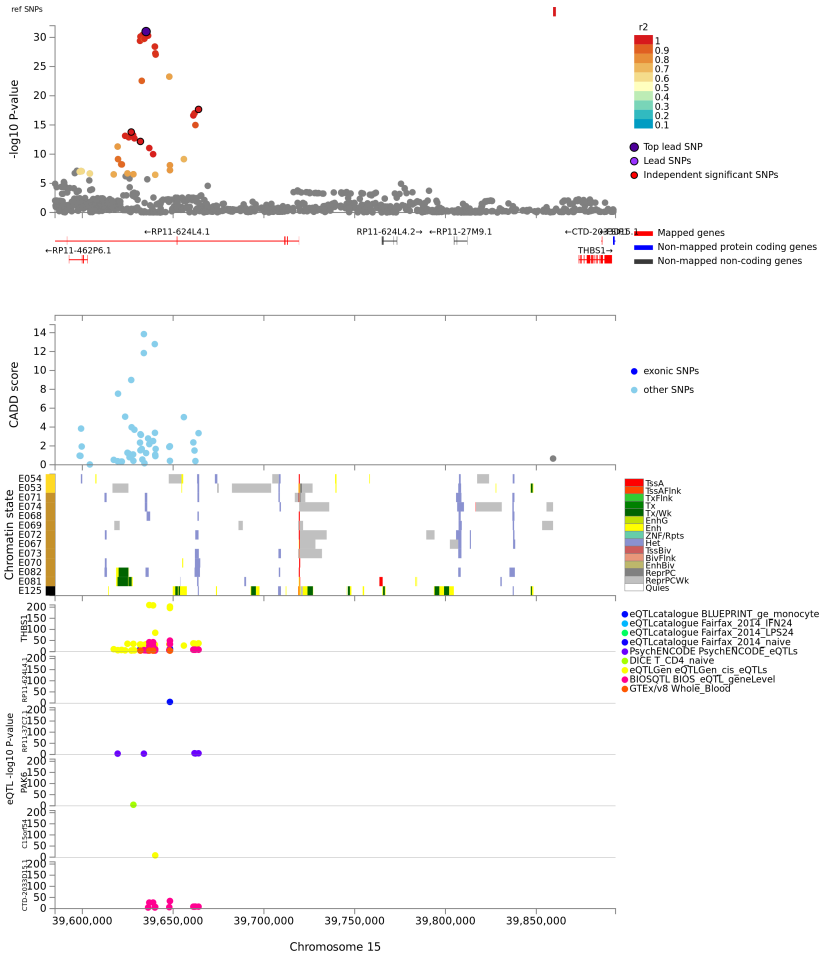

C)

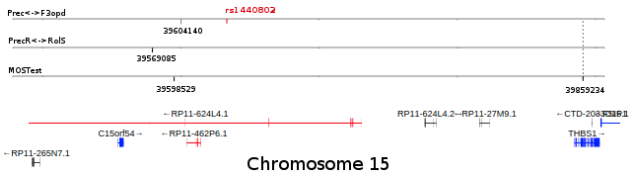

D)

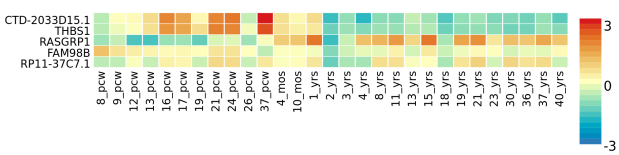

E)

Figure 3: Main results for the 15q14 locus. A) The two pairs of ROIs that forms the endpoints of the associated FCs reported as black bold lines. B) Effect sizes of the SNP rs1440802 for the two connections: (Prec↔F3opd) FC in green and (PrecR↔RolS) FC in yellow. C) Locus Zoom of the genomic region identified by the mvGWAS. Chromatin state of the genomic region. Brain tissue name abbreviations are the following; E054:Ganglion Eminence derived primary cultured neurospheres, E053: Cortex derived primary cultured neurospheres, E071: Brain Hippocampus Middle, E074: Brain Substantia Nigra, E068: Brain Anterior Caudate, E069: Brain Cingulate Gyrus, E072: Brain Inferior Temporal Lobe, E067:Brain Angular Gyrus, E073: Brain Dorsolateral Prefrontal Cortex, E070: Brain Germinal Matrix, E082: Fetal Brain Female, E081: Fetal Brain Male, E125: NH-A Astrocytes Primary Cells. The state abbreviations are the following; TssA: active transcription start site (TSS), TssFlnk: Flanking Active TSS, TxFlnk: Transcription at gene 5′ and 3′, Tx: Strong transcription, TxWk: Weak transcription, EnhG: Genic enhancers, Enh: Enhancers, ZNF/Rpts: ZNF genes & repeats, Het: Heterochromatin, TssBiv: Bivalent/Poised TSS, BivFlnk: Flanking Bivalent TSS/Enh, EnhBiv: Bivalent Enhancer, ReprPC: Repressed PolyComb, ReprPCWk: Weak Repressed PolyComb, Quies: Quiescent/Low. Expression quantitative trait loci (eQTL) associations (data source: eQTLGen (Võsa et al., 2018), PsychENCODE(Wang et al., 2018), DICE (Schmiedel et al., 2018), BIOS QTL browser (Zhernakova et al., 2017), GTEx/v8 (Consortium et al., 2017), eQTLcatalogue). D) Overlap of the genomic region risk region identified from FUMA for MOSTest results, (Prec↔F3opd) and (PrecR↔RolS). E) Gene expression from BrainSpan for the interesting genes prioritised by FUMA.

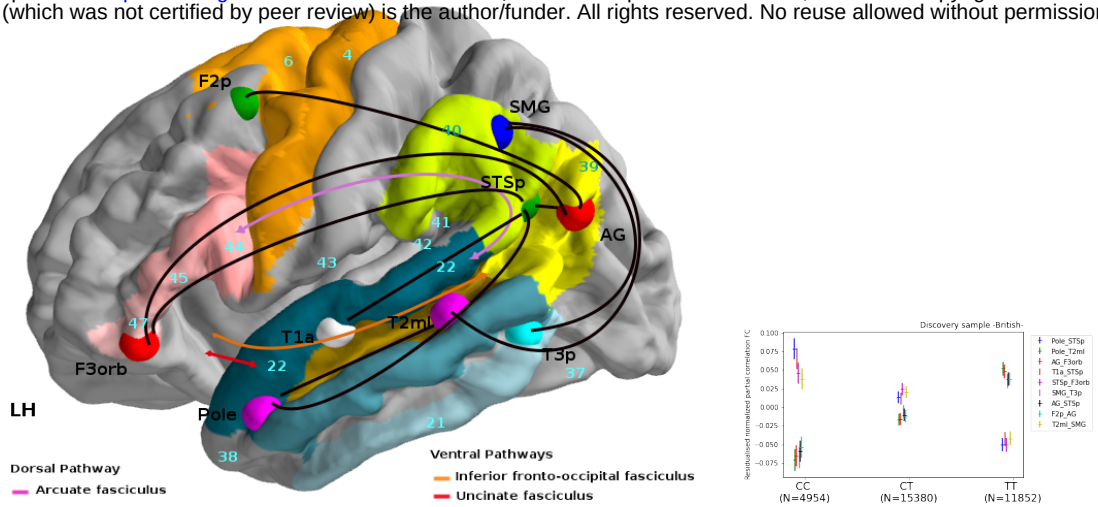

A) B)

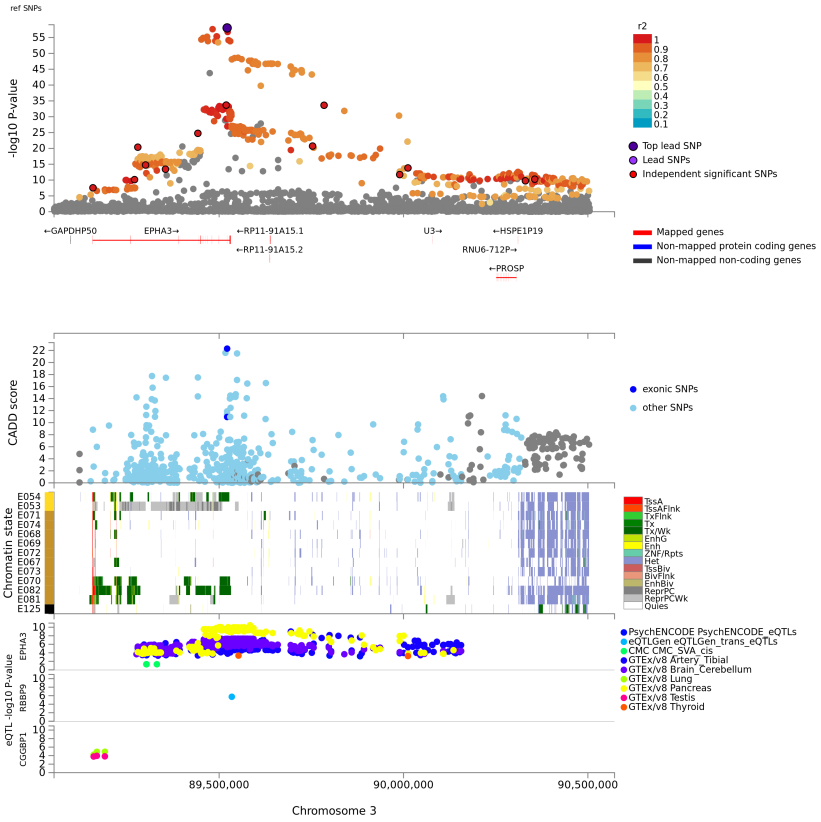

C)

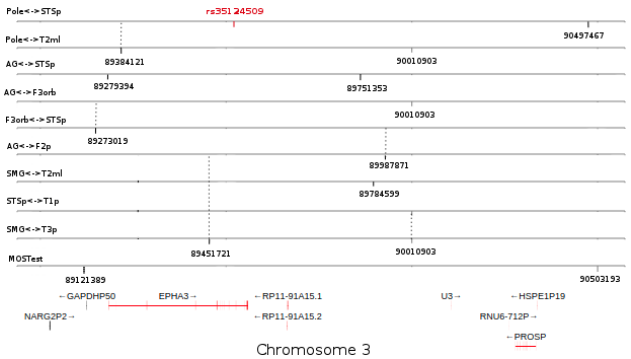

D)

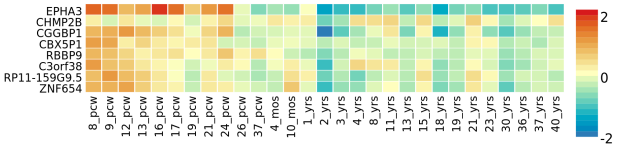

E)

Figure 4: Main results for the 3p11.1 locus. A) The pairs of ROIs that forms the endpoints of the associated FCs reported as black bold lines. B) Effect sizes of the SNP rs35124509 for the nine connections: (AG↔F3orb), (Pole↔STSp), (Pole↔T2ml), (T1a↔STSp), (STSp↔F3orb), (SMG↔T3p), (AG↔STSp), (F2p↔AG) and (T2ml↔SMG) FCs. C) Locus Zoom of the genomic region identified by the mvGWAS. Chromatin state of the genomic region. Brain tissue name abbreviations are the following; E054:Ganglion Eminence derived primary cultured neurospheres, E053: Cortex derived primary cultured neurospheres, E071: Brain Hippocampus Middle, E074: Brain Substantia Nigra, E068: Brain Anterior Caudate, E069: Brain Cingulate Gyrus, E072: Brain Inferior Temporal Lobe, E067:Brain Angular Gyrus, E073: Brain Dorsolateral Prefrontal Cortex, E070: Brain Germinal Matrix, E082: Fetal Brain Female, E081: Fetal Brain Male, E125: NH-A Astrocytes Primary Cells. The state abbreviations are the following; TssA: active transcription start site (TSS), TssFlnk: Flanking Active TSS, TxFlnk: Transcription at gene 5′ and 3′, Tx: Strong transcription, TxWk: Weak transcription, EnhG: Genic enhancers, Enh: Enhancers, ZNF/Rpts: ZNF genes & repeats, Het: Heterochromatin, TssBiv: Bivalent/Poised TSS, BivFlnk: Flanking Bivalent TSS/Enh, EnhBiv: Bivalent Enhancer, ReprPC: Repressed PolyComb, ReprPCWk: Weak Repressed PolyComb, Quies: Quiescent/Low. Expression quantitative trait loci (eQTL) associations (data source: eQTLGen (Võsa et al., 2018), PsychENCODE(Wang et al., 2018), DICE (Schmiedel et al., 2018), BIOS QTL browser (Zhernakova et al., 2017), GTEx/v8 (Consortium et al., 2017), eQTLcatalogue). D) Overlap of the genomic region risk region identified from FUMA for MOSTest results and the nine FCs mentioned above. E) Gene expression from BrainSpan for the interesting genes prioritised by FUMA.

4. Discussion

In this study, we extracted individual language FC endophenotypes from the rsfMRI data of 32,186 participants from the UK Biobank cohort and conducted a multivariate genome-wide association study. We found 4566 significantly associated SNPs distributed over 11 chromosomes. Three multivariate associations with lead SNPs were replicated in the non-British cohort, highlighting the robustness of these signals across different ancestries. Two functional connections, contributing in the *perceptual motor* interaction, associated with 15q14 locus located in the *RP11-624L4.1* antisense gene with modulatory effects on the expression of the *THBS1* gene. Multiple FCs in the *fronto-temporal semantic* language network were found to be associated with SNPs regulating *EPHA3* gene expression in 3p11.1 locus. Each lead SNP was found to be associated with the neuroanatomical white matter tracts that support each of these FCs.

4.1. Locus regulating THBS1 associated with the perceptual motor interactions process

A locus in 15q14 was associated with the precentral-opercularis FC (Prec↔F3opd) and the precentral-Rolandic FC endophenotypes (PrecR↔RolS). The L—R Prec regions in the ventral precentral gyrus are both associated with phonology language component and considered relevant for pharynx and tongue fine-movement coordination in the human and non-human primates (Vigneau et al., 2006; Kumar et al., 2016; Belyk and Brown, 2017). RolS in

the dorsal Rolandic sulcus is attributed to the phonology component and matches the mouth primary motor area but also the perception of syllables (Vigneau et al., 2006; Wilson et al., 2004; Fadiga et al., 2002). F3opd in the dorsal pars opercularis (BA44/45) is associated with semantic/sentence processing. The motor theory of speech perception has been quite an old debate (Liberman and Mattingly, 1985; Galantucci et al., 2006; Flinker et al., 2015; Schwartz et al., 2008; Whalen, 2019). In this study, we report a locus in 15q14 (lead SNP rs1440802) associated with both this FC between the motor and Broca's areas and the frontal aslant tract connecting directly (pre)supplementary motor area with the opercular part of inferior frontal gyrus (Vergani et al., 2014; Catani et al., 2012), in line with this perception–motor link.

SNPs in high LD with rs1440802 in the genomic region have been linked to several other structural features (surface area and cortical thickness) including primary motor cortex, primary somatosensory cortex (Elliott et al., 2018; van der Meer et al., 2020), supramarginal, and pars opercularis (van der Meer et al., 2020), supporting a common genetic influence of the sensory-motor interaction.

The lead SNP rs1440802 and SNPs in LD uncovered to be associated with both (Prec↔F3opd) and (PrecR↔RolS) are found to be eQTL of *THBS1* gene in the blood with high confidence. The thrombospondin-1 protein encoded by *THBS1* gene is a member of the thrombospondin family, a glycoprotein expressed in the extracellular matrix. It has been implicated in synaptogenesis (Christopherson et al., 2005) and regulates the differentiation and proliferation of neural progenitor cells (Lu and Kipnis, 2010), and has been involved in human neocortical evolution (Cáceres et al., 2003, 2007). Other members of the thrombospondin's family, *THBS2* and *THBS4*, have been shown to be over-expressed in the adult human cerebral cortex compared to chimpanzees and macaques (Cáceres et al., 2007). Their increased expression suggests that human brain might display distinctive features involving enhanced synaptic plasticity in adulthood which may contribute to cognitive and linguistic abilities (Sherwood et al., 2008). From a developmental point of view, *THBS1* appears to be un-

der control of temporal expression during development, as revealed by BrainSpan data (See Fig. 3e and Fig. SI4). *THBS1* expression was studied from the longitudinal transcriptomic profile resource of the developing human brain (18, 19, 21, 23 weeks of gestation) (Johnson et al., 2009). Its expression is reported as over-expressed in the neocortex, including the perisylvian language areas, compared to phylogenetically older parts of the brain such as the striatum, thalamus and cerebellum (Johnson et al., 2009). Thrombospondin-1 have been linked to Autism spectrum disorder (Lu et al., 2014), Alzheimer's disease (Ko et al., 2015), and Schizophrenia (Park et al., 2012).

Taken together, these results indicate that *THBS1*, modulated by a lead SNP in the 15q14 locus, could be prioritised in the study of key genes playing a role in the functional connectivity part of the *perceptual motor* interaction required for language, and with the anatomical connectivity, support of their interactions.

4.2. Locus in EPHA3 associated with the fronto-temporal semantic network

A locus in 3p11.1 is found associated with nine fronto-parietal-temporal endophenotypes. The angular gyrus (AG) has been shown to activate during functional imaging tasks probing semantics and involved in conceptual knowledge (Vigneau et al., 2006). F3orb in the pars orbitalis in the inferior frontal gyrus is labelled semantic for its involvement in semantic retrieval in spoken and sign language (Rönnberg et al., 2004). It has also been associated with categorisation, association, and word generation tasks (Noppeney and Price, 2004; Booth et al., 2002; Gurd et al., 2002). The temporal pole region, located in the anterior temporal lobe, is associated with semantic and sentence processing (Vigneau et al., 2006) and the posterior superior temporal sulcus (pSTS) is reported to be implicated in syntactic complexity (Constable et al., 2004) but also process the semantic integration of complex linguistic material (Vigneau et al., 2006). Both pSTS and the angular gyrus overlap with the Geschwind's territory (See Fig. 1a). The lateral/middle part of the middle temporal gyrus is devoted to verbal knowledge (Vigneau et al., 2006). These regions and their corresponding endophenotypes fit rather well with the *fronto-temporal semantic system* described in (Vigneau et al.,

2006) facilitating the association of integrated input messages with internal knowledge. The anterior part of the superior temporal gyrus and the posterior part of the inferior temporal gyrus are phonological–semantic interface areas processing. (Vigneau et al., 2006) propose that these ones are transitional zones between the perception and semantic integration of language stimuli and are crucial during the development of language.

SNPs of this genomic region in high LD with the lead SNP rs35124509 have already been found associated with: rsfMRI ICA functional connectivity (edge 387, 383, 399, and ICA-features 3); see (Elliott et al., 2018). The ICA maps used for these FC estimations partially-overlap semantic language areas including the angular gyrus, the most anterior part of the STS, the anterior fusiform gyrus, the lateral-middle part of T2, the ventral part of the pars triangularis and the pars orbitalis of the left inferior frontal gyrus. Regarding cognitive traits, this locus was associated to intelligence (Savage et al., 2018). Finally, other SNPs, in strong LD with the lead SNP rs35124509, consistently act as an eQTL of *EPHA3* in brain tissues.

The ephrin type-A receptor 3 protein encoded by *EPHA3* gene belongs to the ephrin receptor family that can bind the ephrins subfamily of the tyrosine kinase protein family. EPH receptors and their ligands were found to play important roles in multiple developmental processes, including tissue morphogenesis, embryogenesis, neurogenesis, vascular network formation, neural crest cell migration, axon fasciculation, axon guidance, and topographic neural map formation (Pasquale, 2008; Gibson and Ma, 2011; Gerstmann and Zimmer, 2018). EPHA3 binds predominantly EFNA5 and plays a role in the segregation of motor and sensory axons during neuromuscular circuit development (Lawrenson et al., 2002). In (Johnson et al., 2009), *EPHA3* is reported as over-expressed in the fetal rhesus macaque monkey neocortex (NCTX) and especially in the occipital lobe compared to the other NCTX areas. Noticeably, its ligand *EFNA5* is over-expressed in perisylvian areas and is located in a human accelerated conserved non-coding sequence (haCNS704) (Johnson et al., 2009). EPH receptors have been linked to neurodevelopmental disorders, including schizophrenia (Zhang et al., 2010) and

autism spectrum disorder (Casey et al., 2012). Moreover, in (Rudov et al., 2013), *EPHA3* is found *in silico*, as putative gene implicated in dyspraxia, dyslexia and specific language impairment (SLI). Finally, we observed that *EPHA3* is expressed in the human brain, in a consistent manner across developmental stages from early prenatal to late-mid prenatal (8-24 pcw, BrainSpan ; see Fig. 4e and Fig. SI4).

Taken together, these results indicate that *EPHA3* in the 3p11.1 locus, could be prioritised in the study of key genes playing a role in the *fronto-temporal semantic* network, and with the anatomical connectivity support of this network.

4.3. Locus in PLCE1, NOC3L and HELLS

A locus in 10q23.33 was highlighted by the mvGWAS. At the univariate level, no endophenotype reached the genome-wide significance threshold. But looking at the suggestive threshold $p = 1e-5$, we pinpoint putative 'central' endophenotypes to aid interpretation of the processes underlying this association signal. Two bilateral fronto-temporal endophenotypes were the most associated to rs11187838: the precentral-Rolandic FC endophenotypes (PrecR↔RolS, $p = 1.85e-07$) and the right anterior part of the superior temporal gyrus (T1aR) overlapping Heschl's gyrus (T1a/HeschlR) and its homotopic areas of LH primary auditory regions (T1a↔T1a/HeschlR, $p = 9.61e-06$). All these regions participate in an elementary audio–motor loop involved in both comprehension and production of syllables forming a bilateral fronto-temporal network activated by the auditory representation of speech sounds (Vigneau et al., 2006, 2011). SNPs of this genomic region in high LD with the lead rs11187838 act as an eQTL of *HELLS*, *NOC3L*, *PLCE1* genes in multiple brain tissues (Supplementary Table SI8). The *HELLS* gene encodes the lymphoid-specific helicase (Lsh), a member of the SNF2 helicase family of chromatin remodeling proteins. Patients with a genetic mutation of *HELLS* present psychomotor retardation including slow cognitive, motor development and psychomotor impairment (Thijssen et al., 2015). The Lsh protein might play a role as epigenetic regulator in neural cells (Han et al., 2017). Finally, we observed that the three genes (*NOC3L*, *PLCE1*, *HELLS*) are expressed in the human brain, across

developmental stages from early prenatal to early mid prenatal (8-17 pcw, BrainSpan).

Taken together, these results indicate that the three highlighted genes (*PLCE1*, *NOC3L* and *HELLS*) in the 10q23.33 locus, as potential candidates in the study of key genes playing a role in the *bilateral fronto-temporal auditory-motor* network.

4.4. Limitations

The lack of a large, age-matched replication sample represents one major limitation of the present study in the sense that we could not reproduce all our results. Additionally, we observed that the three associations replicated in the non-British sample were not the three most significant ones. For example, rs2279829 on chr3 was found associated with $p = 7.57\text{e}{-21}$ but was not replicated in the non-British cohort, while rs11187838 on chr10 found associated with $p = 4.29\text{e}{-14}$ was replicated in the non-British cohort with $p = 2.92\text{e}{-2}$. This suggests that some lead SNPs found associated with language FCs with a lower p value than $p = 4.29\text{e}{-14}$ but not replicated in the non-British sample might be specific to the British ancestry. Nevertheless, the sample size of the discovery sample was an order of magnitude larger than the replication sample, making it difficult to compare these different results. Although multivariate methods have shown to substantially increase statistical power and gene discovery compared to univariate approaches, the results are less straightforward to interpret. We have addressed this issue by assessing each of the prioritized loci at the univariate level, to pinpoint at central endophenotypes that are contributing the most to the multivariate signal. Moreover, as such a complex trait as language may be driven by a lot of interacting genes, a multivariate approach on the SNPs side is highly desired to uncover relevant gene pathways in language development and processing. Compared to structural endophenotypes, the FCs have low amplitude which hinders the study in terms of statistical power. This observation constitute a third limitation that is somehow surpassed when working on large scale cohorts and using multivariate approaches. Another potential limitation is the UK Biobank dataset in which this study is based. It should be noted that the UKB constitutes a relatively old sample. Future studies in other developmental stages

(i.e. children, adolescent, young-adult) will inform us whether the observed associations are stable across development, or whether they reflect some age-related specificity.

4.5. Conclusions

Thanks to imaging-genetics modern approaches that allow us to increase in statistical power and circumvent the small effect sizes, we could, at a certain level, shed lights into the genetic architecture of language functional connectivity by highlighting potential key genes related to language processing with -nearly- no recruitment bias. The neurobiology of language, but also many other neuroscience fields, could highly benefit from this type of methodology.

5. Declaration of competing interest

The authors declare that they have no conflict of interest

6. Data Availability

The data used in this study are available via the UK Biobank, `https://www.ukbiobank.ac.uk/`.

7. Ethics statement

UK Biobank dataset: informed consent is obtained from all UK Biobank participants; ethical procedures are controlled by a dedicated Ethics and Guidance Council (http://www.ukbiobank.ac.uk/et that has developed with UK Biobank an Ethics and Governance Framework (given in full at http://www.ukbiobank.ac.uk/wp-content/uploads/2011/05/EGF20082.pdf), with IRB approval also obtained from the North West Multi-center Research Ethics Committee.

8. Code availability

This study used openly available software and codes, specifically GCTA (`https://cnsgenomics.com/software/gcta/#GREML`), PLINK (`http://zzz.bwh.harvard.edu/plink/`), MOSTest

(`https://github.com/precimed/mostest`), and FUMA (`https://fuma.ctglab.nl/`). The anatomical connectivity atlas used is available at (`http://www.bcblab.com/BCB/Atlas_of_Human_Brain_Connections.html`).

9. Acknowledgements

This research was conducted using the UK Biobank resource under application #64984. This project was supported by the Marie Skłodowska-Curie programme awarded to Stephanie J. Forkel (Grant agreement No. 101028551). Amaia Carrion-Castillo was supported by a Juan de la Cierva fellowship from the Spanish Ministry of Science and Innovation, and a Gipuzkoa Fellows fellowship from the Basque Government.

References

Abraham, A., Pedregosa, F., Eickenberg, M., Gervais, P., Mueller, A., Kossaifi, J., Gramfort, A., Thirion, B., Varoquaux, G., 2014. Machine learning for neuroimaging with scikit-learn. Frontiers in Neuroinformatics 8.

Alfaro-Almagro, F., Jenkinson, M., Bangerter, N.K., Andersson, J.L., Griffanti, L., Douaud, G., Sotiropoulos, S.N., Jbabdi, S., Hernandez-Fernandez, M., Vallee, E., et al., 2018. Image processing and quality control for the first 10,000 brain imaging datasets from uk biobank. Neuroimage 166, 400–424.

Ardila, A., Bernal, B., Rosselli, M., 2016. How localized are language brain areas? a review of brodmann areas involvement in oral language. Archives of Clinical Neuropsychology 31, 112–122.

Bates, E., Wilson, S.M., Saygin, A.P., Dick, F., Sereno, M.I., Knight, R.T., Dronkers, N.F., 2003. Voxel-based lesion–symptom mapping. Nature neuroscience 6, 448–450.

Belyk, M., Brown, S., 2017. The origins of the vocal brain in humans. Neuroscience & Biobehavioral Reviews 77, 177–193.

Binder, J.R., Desai, R.H., Graves, W.W., Conant, L.L., 2009. Where is the semantic system? a critical review and meta-analysis of 120 functional neuroimaging studies. Cerebral cortex 19, 2767–2796.

Booth, J.R., Burman, D.D., Meyer, J.R., Gitelman, D.R., Parrish, T.B., Mesulam, M.M., 2002. Modality independence of word comprehension. Human brain mapping 16, 251–261.

Boyle, A.P., Hong, E.L., Hariharan, M., Cheng, Y., Schaub, M.A., Kasowski, M., Karczewski, K.J., Park, J., Hitz, B.C., Weng, S., et al., 2012. Annotation of functional variation in personal genomes using regulomedb. Genome research 22, 1790–1797.

595 Bycroft, C., Freeman, C., Petkova, D., Band, G., Elliott, L.T., Sharp, K., Motyer, A.,
596 Vukcevic, D., Delaneau, O., O'Connell, J., et al., 2018. The uk biobank resource with deep
597 phenotyping and genomic data. Nature 562, 203–209.

598 Cáceres, M., Lachuer, J., Zapala, M.A., Redmond, J.C., Kudo, L., Geschwind, D.H., Lock-
599 hart, D.J., Preuss, T.M., Barlow, C., 2003. Elevated gene expression levels distinguish
600 human from non-human primate brains. Proceedings of the National Academy of Sciences
601 100, 13030–13035.

602 Cáceres, M., Suwyn, C., Maddox, M., Thomas, J.W., Preuss, T.M., 2007. Increased corti-
603 cal expression of two synaptogenic thrombospondins in human brain evolution. Cerebral
604 Cortex 17, 2312–2321.

605 Casey, J.P., Magalhaes, T., Conroy, J.M., Regan, R., Shah, N., Anney, R., Shields, D.C.,
606 Abrahams, B.S., Almeida, J., Bacchelli, E., et al., 2012. A novel approach of homozygous
607 haplotype sharing identifies candidate genes in autism spectrum disorder. Human genetics
608 131, 565–579.

609 Catani, M., De Schotten, M.T., 2008. A diffusion tensor imaging tractography atlas for
610 virtual in vivo dissections. cortex 44, 1105–1132.

611 Catani, M., Dell'Acqua, F., Vergani, F., Malik, F., Hodge, H., Roy, P., Valabregue, R.,
612 De Schotten, M.T., 2012. Short frontal lobe connections of the human brain. cortex 48,
613 273–291.

614 Catani, M., Forkel, S.J., 2019. Diffusion imaging methods in language sciences. The Oxford
615 Handbook of Neurolinguistics , 212.

616 Catani, M., Jones, D.K., Ffytche, D.H., 2005. Perisylvian language networks of the human
617 brain. Annals of Neurology: Official Journal of the American Neurological Association and
618 the Child Neurology Society 57, 8–16.

Chang, C.C., Chow, C.C., Tellier, L.C., Vattikuti, S., Purcell, S.M., Lee, J.J., 2015. Second-generation plink: rising to the challenge of larger and richer datasets. Gigascience 4, s13742–015.

Christopherson, K.S., Ullian, E.M., Stokes, C.C., Mullowney, C.E., Hell, J.W., Agah, A., Lawler, J., Mosher, D.F., Bornstein, P., Barres, B.A., 2005. Thrombospondins are astrocyte-secreted proteins that promote cns synaptogenesis. Cell 120, 421–433.

Cirnaru, M.D., Song, S., Tshilenge, K.T., Corwin, C., Mleczko, J., Aguirre, C.G., Benlhabib, H., Bendl, J., Fullard, J., Apontes, P., et al., 2020. Transcriptional and epigenetic characterization of early striosomes identifies foxf2 and olig2 as factors required for development of striatal compartmentation and neuronal phenotypic differentiation. bioRxiv .

Cole, M.W., Ito, T., Bassett, D.S., Schultz, D.H., 2016. Activity flow over resting-state networks shapes cognitive task activations. Nature neuroscience 19, 1718–1726.

Consortium, G., et al., 2017. Genetic effects on gene expression across human tissues. Nature 550, 204–213.

Constable, R.T., Pugh, K.R., Berroya, E., Mencl, W.E., Westerveld, M., Ni, W., Shankweiler, D., 2004. Sentence complexity and input modality effects in sentence comprehension: an fmri study. NeuroImage 22, 11–21.

Daducci, A., Canales-Rodríguez, E.J., Zhang, H., Dyrby, T.B., Alexander, D.C., Thiran, J.P., 2015. Accelerated microstructure imaging via convex optimization (amico) from diffusion mri data. NeuroImage 105, 32–44.

Dohmatob, E., Richard, H., Pinho, A.L., Thirion, B., 2021. Brain topography beyond parcellations: Local gradients of functional maps. NeuroImage 229.

Dubois, J., Adolphs, R., 2016. Building a science of individual differences from fmri. Trends in cognitive sciences 20, 425–443.

643 Elliott, L.T., Sharp, K., Alfaro-Almagro, F., Shi, S., Miller, K.L., Douaud, G., Marchini, J.,
644 Smith, S.M., 2018. Genome-wide association studies of brain imaging phenotypes in uk
645 biobank. Nature 562, 210–216.

646 Ernst, J., Kellis, M., 2012. Chromhmm: automating chromatin-state discovery and charac-
647 terization. Nature methods 9, 215–216.

648 Fadiga, L., Craighero, L., Buccino, G., Rizzolatti, G., 2002. Speech listening specifically mod-
649 ulates the excitability of tongue muscles: a tms study. European journal of Neuroscience
650 15, 399–402.

651 Fedorenko, E., 2021. The early origins and the growing popularity of the individual-subject
652 analytic approach in human neuroscience. Current Opinion in Behavioral Sciences 40,
653 105–112.

654 Fisher, S.E., Vargha-Khadem, F., Watkins, K.E., Monaco, A.P., Pembrey, M.E., 1998. Lo-
655 calisation of a gene implicated in a severe speech and language disorder. Nature genetics
656 18, 168–170.

657 Fisher, S.E., Vernes, S.C., 2015. Genetics and the language sciences. Annu. Rev. Linguist.
658 1, 289–310.

659 Flinker, A., Korzeniewska, A., Shestyuk, A.Y., Franaszczuk, P.J., Dronkers, N.F., Knight,
660 R.T., Crone, N.E., 2015. Redefining the role of broca's area in speech. Proceedings of the
661 National Academy of Sciences 112, 2871–2875.

662 Forkel, S., Catani, M., 2018. Structural Neuroimaging. pp. 288–308.

663 Forkel, S.J., Friedrich, P., Thiebaut de Schotten, M., Howells, H., 2020a. White matter
664 variability, cognition, and disorders: a systematic review .

665 Forkel, S.J., Rogalski, E., Sancho, N.D., D'Anna, L., Laguna, P.L., Sridhar, J., Dell'Acqua,

F., Weintraub, S., Thompson, C., Mesulam, M.M., et al., 2020b. Anatomical evidence of an indirect pathway for word repetition. Neurology 94, e594–e606.

Forkel, S.J., Thiebaut de Schotten, M., Dell'Acqua, F., Kalra, L., Murphy, D.G., Williams, S.C., Catani, M., 2014a. Anatomical predictors of aphasia recovery: a tractography study of bilateral perisylvian language networks. Brain 137, 2027–2039.

Forkel, S.J., de Schotten, M.T., Kawadler, J.M., Dell'Acqua, F., Danek, A., Catani, M., 2014b. The anatomy of fronto-occipital connections from early blunt dissections to contemporary tractography. Cortex 56, 73–84.

Fridriksson, J., Moser, D., Ryalls, J., Bonilha, L., Rorden, C., Baylis, G., 2009. Modulation of frontal lobe speech areas associated with the production and perception of speech movements .

Friederici, A.D., 2011. The brain basis of language processing: from structure to function. Physiological reviews 91, 1357–1392.

Friederici, A.D., 2017. Language in our brain: The origins of a uniquely human capacity. MIT Press.

Galantucci, B., Fowler, C.A., Turvey, M.T., 2006. The motor theory of speech perception reviewed. Psychonomic bulletin & review 13, 361–377.

Gerstmann, K., Zimmer, G., 2018. The role of the eph/ephrin family during cortical development and cerebral malformations. Medical Research Archives 6.

Gibson, D.A., Ma, L., 2011. Developmental regulation of axon branching in the vertebrate nervous system. Development 138, 183–195.

Gurd, J.M., Amunts, K., Weiss, P.H., Zafiris, O., Zilles, K., Marshall, J.C., Fink, G.R., 2002. Posterior parietal cortex is implicated in continuous switching between verbal fluency tasks: an fmri study with clinical implications. Brain 125, 1024–1038.

690 Han, Y., Ren, J., Lee, E., Xu, X., Yu, W., Muegge, K., 2017. Lsh/hells regulates self-
691 renewal/proliferation of neural stem/progenitor cells. Scientific reports 7, 1–14.

692 Jackendoff, R., Jackendoff, R.S., 2002. Foundations of language: Brain, meaning, grammar,
693 evolution. Oxford University Press, USA.

694 Jackson, R.L., Hoffman, P., Pobric, G., Ralph, M.A.L., 2016. The semantic network at
695 work and rest: differential connectivity of anterior temporal lobe subregions. Journal of
696 Neuroscience 36, 1490–1501.

697 Johnson, M.B., Kawasawa, Y.I., Mason, C.E., Krsnik, Ž., Coppola, G., Bogdanović, D.,
698 Geschwind, D.H., Mane, S.M., State, M.W., Šestan, N., 2009. Functional and evolutionary
699 insights into human brain development through global transcriptome analysis. Neuron 62,
700 494–509.

701 Kircher, M., Witten, D.M., Jain, P., O'Roak, B.J., Cooper, G.M., Shendure, J., 2014. A
702 general framework for estimating the relative pathogenicity of human genetic variants.
703 Nature genetics 46, 310–315.

704 Ko, C.Y., Chu, Y.Y., Narumiya, S., Chi, J.Y., Furuyashiki, T., Aoki, T., Wang,
705 S.M., Chang, W.C., Wang, J.M., 2015. The ccaat/enhancer-binding protein
706 delta/mir135a/thrombospondin 1 axis mediates pge2-induced angiogenesis in alzheimer's
707 disease. Neurobiology of aging 36, 1356–1368.

708 Kumar, V., Croxson, P.L., Simonyan, K., 2016. Structural organization of the laryngeal
709 motor cortical network and its implication for evolution of speech production. Journal of
710 Neuroscience 36, 4170–4181.

711 Labache, L., Mazoyer, B., Joliot, M., Crivello, F., Hesling, I., Tzourio-Mazoyer, N., 2020.
712 Typical and atypical language brain organization based on intrinsic connectivity and mul-
713 titask functional asymmetries. eLife 9, 1–31.

Landi, N., Perdue, M.V., 2019. Neuroimaging genetics studies of specific reading disability and developmental language disorder: A review. Language and linguistics compass 13, e12349.

Lawrenson, I.D., Wimmer-Kleikamp, S.H., Lock, P., Schoenwaelder, S.M., Down, M., Boyd, A.W., Alewood, P.F., Lackmann, M., 2002. Ephrin-a5 induces rounding, blebbing and de-adhesion of epha3-expressing 293t and melanoma cells by crkii and rho-mediated signalling. Journal of cell science 115, 1059–1072.

Ledoit, O., Wolf, M., 2004. A well-conditioned estimator for large-dimensional covariance matrices. Journal of multivariate analysis 88, 365–411.

Lee, S.H., Yang, J., Goddard, M.E., Visscher, P.M., Wray, N.R., 2012. Estimation of pleiotropy between complex diseases using single-nucleotide polymorphism-derived genomic relationships and restricted maximum likelihood. Bioinformatics 28, 2540–2542.

Leroy, F., Cai, Q., Bogart, S.L., Dubois, J., Coulon, O., Monzalvo, K., Fischer, C., Glasel, H., Van der Haegen, L., Bénézit, A., Lin, C.P., Kennedy, D.N., Ihara, A.S., Hertz-Pannier, L., Moutard, M.L., Poupon, C., Brysbaert, M., Roberts, N., Hopkins, W.D., Mangin, J.F., Dehaene-Lambertz, G., 2015. New human-specific brain landmark: The depth asymmetry of superior temporal sulcus. Proceedings of the National Academy of Sciences , 201412389.

Liberman, A.M., Mattingly, I.G., 1985. The motor theory of speech perception revised. Cognition 21, 1–36.

Lu, L., Guo, H., Peng, Y., Xun, G., Liu, Y., Xiong, Z., Tian, D., Liu, Y., Li, W., Xu, X., et al., 2014. Common and rare variants of the thbs1 gene associated with the risk for autism. Psychiatric genetics 24, 235–240.

Lu, Z., Kipnis, J., 2010. Thrombospondin 1—a key astrocyte-derived neurogenic factor. The FASEB Journal 24, 1925–1934.

738 Marrelec, G., Krainik, A., Duffau, H., Pélégrini-Issac, M., Lehéricy, S., Doyon, J., Benali, H.,
739 2006. Partial correlation for functional brain interactivity investigation in functional mri.
740 Neuroimage 32, 228–237.

741 van der Meer, D., Frei, O., Kaufmann, T., Shadrin, A.A., Devor, A., Smeland, O.B., Thomp-
742 son, W.K., Fan, C.C., Holland, D., Westlye, L.T., et al., 2020. Understanding the genetic
743 determinants of the brain with mostest. Nature communications 11, 1–9.

744 Miller, K.L., Alfaro-Almagro, F., Bangerter, N.K., Thomas, D.L., Yacoub, E., Xu, J.,
745 Bartsch, A.J., Jbabdi, S., Sotiropoulos, S.N., Andersson, J.L., et al., 2016. Multimodal
746 population brain imaging in the uk biobank prospective epidemiological study. Nature
747 neuroscience 19, 1523–1536.

748 Ngo, G.H., Khosla, M., Jamison, K., Kuceyeski, A., Sabuncu, M.R., 2020. From Connectomic
749 to Task-evoked Fingerprints: Individualized Prediction of Task Contrasts from Resting-
750 state Functional Connectivity. Lecture Notes in Computer Science (including subseries
751 Lecture Notes in Artificial Intelligence and Lecture Notes in Bioinformatics) 12267 LNCS,
752 62–71. 2008.02961.

753 Nishitani, N., Hari, R., 2000. Temporal dynamics of cortical representation for action. Pro-
754 ceedings of the National Academy of Sciences 97, 913–918.

755 Noppeney, U., Price, C.J., 2004. Retrieval of abstract semantics. Neuroimage 22, 164–170.

756 Park, H.J., Kim, S.K., Kim, J.W., Kang, W.S., Chung, J.H., 2012. Association of throm-
757 bospondin 1 gene with schizophrenia in korean population. Molecular biology reports 39,
758 6875–6880.

759 Pasquale, E.B., 2008. Eph-ephrin bidirectional signaling in physiology and disease. Cell 133,
760 38–52.

761 Popp, N.A., Yu, D., Green, B., Chew, E.Y., Ning, B., Chan, C.C., Tuo, J., 2016. Functional
762 single nucleotide polymorphism in il- 17 a 3' untranslated region is targeted by mi r-4480

763 in vitro and may be associated with age-related macular degeneration. Environmental and
764 molecular mutagenesis 57, 58–64.

765 Price, C.J., 2012. A review and synthesis of the first 20 years of pet and fmri studies of heard
766 speech, spoken language and reading. Neuroimage 62, 816–847.

767 Purcell, S., Neale, B., Todd-Brown, K., Thomas, L., Ferreira, M.A., Bender, D., Maller,
768 J., Sklar, P., De Bakker, P.I., Daly, M.J., et al., 2007. Plink: a tool set for whole-
769 genome association and population-based linkage analyses. The American journal of human
770 genetics 81, 559–575.

771 Qi, T., Wu, Y., Zeng, J., Zhang, F., Xue, A., Jiang, L., Zhu, Z., Kemper, K., Yengo, L.,
772 Zheng, Z., et al., 2018. Identifying gene targets for brain-related traits using transcriptomic
773 and methylomic data from blood. Nature communications 9, 1–12.

774 Ramasamy, A., Trabzuni, D., Guelfi, S., Varghese, V., Smith, C., Walker, R., De, T., Coin,
775 L., De Silva, R., Cookson, M.R., et al., 2014. Genetic variability in the regulation of gene
776 expression in ten regions of the human brain. Nature neuroscience 17, 1418–1428.

777 Ramensky, V., Bork, P., Sunyaev, S., 2002. Human non-synonymous snps: server and survey.
778 Nucleic acids research 30, 3894–3900.

779 Rojkova, K., Volle, E., Urbanski, M., Humbert, F., Dell'Acqua, F., De Schotten, M.T., 2016.
780 Atlasing the frontal lobe connections and their variability due to age and education: a
781 spherical deconvolution tractography study. Brain Structure and Function 221, 1751–1766.

782 Rönnberg, J., Rudner, M., Ingvar, M., 2004. Neural correlates of working memory for sign
783 language. Cognitive Brain Research 20, 165–182.

784 Rudov, A., Rocchi, M.B.L., Accorsi, A., Spada, G., Procopio, A.D., Olivieri, F., Rippo,
785 M.R., Albertini, M.C., 2013. Putative mirnas for the diagnosis of dyslexia, dyspraxia, and
786 specific language impairment. Epigenetics 8, 1023–1029.

787 Savage, J.E., Jansen, P.R., Stringer, S., Watanabe, K., Bryois, J., De Leeuw, C.A., Nagel,
788 M., Awasthi, S., Barr, P.B., Coleman, J.R., et al., 2018. Genome-wide association meta-
789 analysis in 269,867 individuals identifies new genetic and functional links to intelligence.
790 Nature genetics 50, 912–919.

791 Schmiedel, B.J., Singh, D., Madrigal, A., Valdovino-Gonzalez, A.G., White, B.M., Zapardiel-
792 Gonzalo, J., Ha, B., Altay, G., Greenbaum, J.A., McVicker, G., et al., 2018. Impact of
793 genetic polymorphisms on human immune cell gene expression. Cell 175, 1701–1715.

794 Schwartz, J.L., Basirat, A., Ménard, L., Sato, M., 2012. The perception-for-action-control
795 theory (pact): A perceptuo-motor theory of speech perception. Journal of Neurolinguistics
796 25, 336–354.

797 Schwartz, J.L., Sato, M., Fadiga, L., 2008. The common language of speech perception and
798 action: a neurocognitive perspective. Revue française de linguistique appliquée 13, 9–22.

799 Seghier, M.L., Price, C.J., 2018. Interpreting and utilising intersubject variability in brain
800 function. Trends in cognitive sciences 22, 517–530.

801 Sherwood, C.C., Subiaul, F., Zawidzki, T.W., 2008. A natural history of the human mind:
802 tracing evolutionary changes in brain and cognition. Journal of anatomy 212, 426–454.

803 Smith, S.M., Fox, P.T., Miller, K.L., Glahn, D.C., Fox, P.M., Mackay, C.E., Filippini, N.,
804 Watkins, K.E., Toro, R., Laird, A.R., et al., 2009. Correspondence of the brain's functional
805 architecture during activation and rest. Proceedings of the national academy of sciences
806 106, 13040–13045.

807 Sudlow, C., Gallacher, J., Allen, N., Beral, V., Burton, P., Danesh, J., Downey, P., Elliott, P.,
808 Green, J., Landray, M., et al., 2015. Uk biobank: an open access resource for identifying the
809 causes of a wide range of complex diseases of middle and old age. Plos med 12, e1001779.

Tavor, I., Jones, O.P., Mars, R., Smith, S., Behrens, T., Jbabdi, S., 2016. Task-free mri predicts individual differences in brain activity during task performance. Science 352, 216–220.

Thijssen, P.E., Ito, Y., Grillo, G., Wang, J., Velasco, G., Nitta, H., Unoki, M., Yoshihara, M., Suyama, M., Sun, Y., et al., 2015. Mutations in cdca7 and hells cause immunodeficiency–centromeric instability–facial anomalies syndrome. Nature communications 6, 1–8.

Turner, T.H., Fridriksson, J., Baker, J., Eoute Jr, D., Bonilha, L., Rorden, C., 2009. Obligatory broca's area modulation associated with passive speech perception. Neuroreport 20, 492.

Uddén, J., Hultén, A., Bendtz, K., Mineroff, Z., Kucera, K.S., Vino, A., Fedorenko, E., Hagoort, P., Fisher, S.E., 2019. Toward robust functional neuroimaging genetics of cognition. Journal of Neuroscience 39, 8778–8787.

Vergani, F., Lacerda, L., Martino, J., Attems, J., Morris, C., Mitchell, P., de Schotten, M.T., Dell'Acqua, F., 2014. White matter connections of the supplementary motor area in humans. Journal of Neurology, Neurosurgery & Psychiatry 85, 1377–1385.

Vigneau, M., Beaucousin, V., Herve, P.Y., Duffau, H., Crivello, F., Houde, O., Mazoyer, B., Tzourio-Mazoyer, N., 2006. Meta-analyzing left hemisphere language areas: phonology, semantics, and sentence processing. Neuroimage 30, 1414–1432.

Vigneau, M., Beaucousin, V., Hervé, P.Y., Jobard, G., Petit, L., Crivello, F., Mellet, E., Zago, L., Mazoyer, B., Tzourio-Mazoyer, N., 2011. What is right-hemisphere contribution to phonological, lexico-semantic, and sentence processing?: Insights from a meta-analysis. Neuroimage 54, 577–593.

Võsa, U., Claringbould, A., Westra, H.J., Bonder, M.J., Deelen, P., Zeng, B., Kirsten, H., Saha, A., Kreuzhuber, R., Kasela, S., et al., 2018. Unraveling the polygenic architecture of complex traits using blood eqtl metaanalysis. BioRxiv , 447367.

Wain, L.V., Shrine, N., Miller, S., Jackson, V.E., Ntalla, I., Artigas, M.S., Billington, C.K., Kheirallah, A.K., Allen, R., Cook, J.P., et al., 2015. Novel insights into the genetics of smoking behaviour, lung function, and chronic obstructive pulmonary disease (uk bileve): a genetic association study in uk biobank. The Lancet Respiratory Medicine 3, 769–781.

Wang, D., Liu, S., Warrell, J., Won, H., Shi, X., Navarro, F.C., Clarke, D., Gu, M., Emani, P., Yang, Y.T., et al., 2018. Comprehensive functional genomic resource and integrative model for the human brain. Science 362.

Wang, K., Li, M., Hakonarson, H., 2010. Annovar: functional annotation of genetic variants from high-throughput sequencing data. Nucleic acids research 38, e164–e164.

Watanabe, K., Taskesen, E., Van Bochoven, A., Posthuma, D., 2017. Functional mapping and annotation of genetic associations with fuma. Nature communications 8, 1–11.

Westra, H.J., Peters, M.J., Esko, T., Yaghootkar, H., Schurmann, C., Kettunen, J., Christiansen, M.W., Fairfax, B.P., Schramm, K., Powell, J.E., et al., 2013. Systematic identification of trans eqtls as putative drivers of known disease associations. Nature genetics 45, 1238–1243.

Whalen, D., 2019. The motor theory of speech perception, in: Oxford Research Encyclopedia of Linguistics.

Wilson, S.M., Saygin, A.P., Sereno, M.I., Iacoboni, M., 2004. Listening to speech activates motor areas involved in speech production. Nature neuroscience 7, 701–702.

Yang, J., Benyamin, B., McEvoy, B.P., Gordon, S., Henders, A.K., Nyholt, D.R., Madden, P.A., Heath, A.C., Martin, N.G., Montgomery, G.W., Goddard, M.E., Visscher, P.M., 2010. Common snps explain a large proportion of the heritability for human height. Nature genetics 42, 565–569. Cited By :2294.

Yang, J., Lee, S.H., Goddard, M.E., Visscher, P.M., 2011. Gcta: a tool for genome-wide complex trait analysis. The American Journal of Human Genetics 88, 76–82.

860 Zhang, H., Schneider, T., Wheeler-Kingshott, C.A., Alexander, D.C., 2012. Noddi: practical
861 in vivo neurite orientation dispersion and density imaging of the human brain. Neuroimage
862 61, 1000–1016.

863 Zhang, R., Zhong, N.N., Liu, X.G., Yan, H., Qiu, C., Han, Y., Wang, W., Hou, W.K., Liu, Y.,
864 Gao, C.G., et al., 2010. Is the efnb2 locus associated with schizophrenia? single nucleotide
865 polymorphisms and haplotypes analysis. Psychiatry research 180, 5–9.

866 Zhernakova, D.V., Deelen, P., Vermaat, M., Van Iterson, M., Van Galen, M., Arindrarto,
867 W., Van't Hof, P., Mei, H., Van Dijk, F., Westra, H.J., et al., 2017. Identification of
868 context-dependent expression quantitative trait loci in whole blood. Nature genetics 49,
869 139–145.

10. Tables

Table 1: Genomic loci associated highlighted using the multivariate genome-wide association studie. Lead SNP: ID of the lead SNPs within each locus. Position: position of the SNP in the hg19 human reference genome. mvgwasP discovery -British-: MOSTest association P value obtained using the discovery sample. mvgwasP replication -non British-: MOSTest association P value obtained using the independent replication sample. Functionnal category: Functional consequence of the SNP on the gene obtained from ANNOVAR. 'Central' phenotypes: the phenotypes that contributed most to the multivariate association considering the genome-wide association threshold ($5e-8$).

Genomic Locus	Lead SNP	Chr	Position	Functional Category	non effect allele	effect allele	MAF	mvgwasP (discovery -British-)	mvgwasP (replication -non British-)	Nearest Gene	'central' phenotypes
1	rs62141276	2	48214217	ncRNA intronic	A	G	0.367	$p = 3.26e{-9}$	$p = 0.27$	*AC079807.4*	-
2	rs2717046	2	58041936	intergenic	T	C	0.380	$p = 7.50e{-14}$	$p = 0.95$	*CTD-2026C7.1*	-
3	rs62158166	2	114077218	intergenic	C	G	0.223	$p = 8.69e{-10}$	$p = 0.38$	*PAX8*	-
4	rs67851870	3	17554860	intronic	G	A	0.322	$p = 6.57e{-16}$	$p = 0.35$	*TBC1D5*	-
5	**rs35124509**	**3**	**89521693**	**exonic**	**C**	**T**	**0.401**	$\mathbf{p = 8.95e{-59}}$	$\mathbf{p = 3.25e{-3}}$	***EPHA3***	**AG↔F3orb,pSTS↔Pole, Pole↔T2ml,T1a↔STSp STSp↔F3orb,SMG↔T3p, AG↔STSp,F2p↔AG, T2ml↔SMG**
6	rs62266110	3	93537923	intergenic	A	G	0.319	$p = 1.17e{-09}$	$p = 0.93$	*RNU6-488P*	-
7	rs2279829	3	147106319	UTR3	T	C	0.212	$p = 7.57e{-21}$	$p = 0.68$	*ZIC4*	-
8	rs145120402	5	93174765	intronic	C	A	0.0433	$p = 1.83e{-9}$	$p = 0.10$	*FAM172A*	-
9	5:94068140_AC_A	5	94068140	intronic	A	AC	0.209	$p = 6.79e{-9}$	$p = 0.30$	*ANKRD32:MCTP1*	-
10	rs4262195	6	96929475	ncRNA intronic	C	T	0.181	$p = 7.19e{-9}$	$p = 0.70$	*UFL1-AS1*	-
11	**rs11187838**	**10**	**96038686**	**intronic**	**A**	**G**	**0.435**	$\mathbf{p = 4.29e{-14}}$	$\mathbf{p = 2.92e{-2}}$	***PLCE1***	**-**
12	rs11146399	10	134308479	intergenic	T	C	0.457	$p = 5.50e{-16}$	$p = 0.28$	*RP11-432J24.5*	-
13	rs11218557	11	122099839	ncRNA intronic	C	T	0.4579	$p = 1.24e{-8}$	$p = 0.77$	*RP11-820L6.1*	-
14	rs186347	14	59072226	intergenic	T	G	0.458	$p = 2.08e{-11}$	$p = 0.92$	*DACT1*	-
15	**rs1440802**	**15**	**39635124**	**ncRNA intronic**	**C**	**T**	**0.090**	$\mathbf{p = 1e{-31}}$	$\mathbf{p = 9.58e{-3}}$	***RP11-624L4.1***	**Prec↔F3opd, PrecR↔RolS**
16	rs4702	15	91426560	UTR3	A	G	0.442	$p = 3.77e{-13}$	$p = 0.42$	*FURIN*	-
17	rs34039488	17	27320232	intronic	A	G	0.162	$p = 4.74e{-8}$	$p = 0.46$	*PIPOX:SEZ6*	-
18	17:44270659_G_A	17	44270659	intronic	A	G	0.399	$p = 5.36e{-16}$	$p = 0.45$	*KANSL1*	-
19	rs7234875	18	73114340	intergenic	C	T	0.399	$p = 5.71e{-14}$	$p = 0.82$	*RP11-321M21.3*	-
20	rs2542028	22	47196524	intronic	G	A	0.268	$p = 3.06e{-12}$	$p = 0.60$	*TBC1D22A*	-

Supplementary tables (separate Excel file)

Table SI1: Overview of the regions obtained from the meta-analysis. Each ROIs is characterized by their abbreviated anatomical label defined by Vigneau et al. (2006, 2011) and is labelled according to the language component they belong to : phonology, semantic, and syntax.

Table SI2: Heritabilities of the 300 brain functional connectivity, estimated using the genotyped SNPs information using genome-based restricted maximum likelihood (GREML) (Yang et al., 2010) as implemented in GCTA (Yang et al., 2011) software (version 1.93.2beta). A 0.05 threshold on False Discovery Rate (FDR) adjusted p-values was applied to account for multiple testing.

Table SI3: SNPs associated with the 142 heritable functional connectivity measures using MOSTest (van der Meer et al., 2020) at the genome-wide significance threshold $p = 5e{-}8$.

Table SI4: Replication of the 20 lead SNP association using an independent non-British replication dataset (N=4,754) using MOSTest (van der Meer et al., 2020). We considered the nominal significance threshold $pvalue < 0.05$.

Table SI5: For each of the 20 lead SNPs identified in the multivariate GWAS, the corresponding univariate summary statistics for FCs identified as central FC (threshold on the genome-wide significance threshold $p = 5e{-}8$).

Table SI6: The SNP-based genetic correlation analysis was estimated (using GCTA (Lee et al., 2012) software, version 1.93.2beta) for each pair of central FCs associated to 15q14 or 3p11.1 genetic loci.

Table SI7: Univariate associations of 2 lead SNPs (rs1440802 on 15q14, rs35124509 on 3p11.1) using PLINK 1.9 (Purcell et al., 2007) with diffusion MRI indices on the following 7 white matter tracts: the corpus callosum, the left frontal aslant tract, the left arcuate anterior/long/posterior segment, the left inferior fronto-occipital fasciculus, the left uncinate tract. Significant results were considered at the Bonferroni-corrected threshold $p = 6.94e{-}3 (0.05/(3 * 9 + 5 * 9))$.

Table SI8: eQTLs association, performed by FUMA, between the SNPs in the three replicated genomic risk loci and all mapped genes in the following databases : GTEx/v8 (Consortium et al., 2017), PsychENCODE (Wang et al., 2018), eQTLGen (Võsa et al., 2018), eQTLcatalogue, DICE (Schmiedel et al., 2018), BIOSQTL (Zhernakova et al., 2017). A 0.05 threshold on False Discovery Rate (FDR) adjusted p-values was applied to account for multiple testing.

Table SI9: Center of mass of the language processing regions of interests retained in both left and right hemispheres. Each ROIs is characterised by their abbreviated anatomical label defined by (Vigneau et al., 2006, 2011) and their center of mass MNI stereotactic coordinates (x, y, z, in mm).

11. Supplementary figures

Figure SI1: Locus Zoom of the significant loci identified by the multiariate GWAS for functional connectivity.

Figure SI2: **Genomic loci, eQTL associations and chromatin interactions identified via multivariate GWAS for functional connectivity.** Circos plot representing the genomic risk loci, and the genes associated with the loci by chromatin interactions and eQTLs. From outer layer to inner layer: Manhattan plot. Genomic risk loci are in blue. Genes mapped by chromatin interaction are in orange. Genes mapped by eQTL are in green. Genes mapped by both are in red. Chromatin interaction and eQTLs links follows the same color coding presented above.

Figure SI3: **Regional effects.** Circle plot illustrating the lead SNPs identified from the multivariate GWAS for functional connectivity. Z-values from the univariate GWAS for each FCs are mapped. The absolute Z-values scaling is clipped at 8 ($p = 1.2\text{e}{-15}$). Positif effects of carrying the minor allele are shown in red, and negative in blue.

Figure SI4: **Functional annotation of both genomic risk loci 15q14 and 3p11.1.** A) Gene expression heatmap constructed with GTEx/v8 (54 tissue types) and B) BrainSpan 29 different ages of brain samples. (Average of normalized expression per label).